Journal of Mechanical Engineering Research and Developments
ISSN: 1024-1752
CODEN: JERDFO
Vol. 43, No. 6, pp. 487-496
Published Year 2020

Laser Powder Bed Fusion: Evaluation of Ti15Mo single tracks

Thywill Cephas Dzogbewu*

Department of Mechanical and Mechatronics Engineering Central University of Technology, Free State, Bloemfontein, South Africa.

*Corresponding author email: thydzo@yahoo.fr

ABSTRACT: The laser powder bed fusion (LPBF) process could be used to manufacture 3D objects from elemental powders layer-by-layer using single tracks. However, it is required to determine the optimum process parameters for each type of powder blend and composition that could be used to produce the single tracks for the subsequent manufacturing of the 3D object. The current investigation determined the optimum process parameter window for the Ti15Mo powder blend using the LPBF process. Single tracks were produced at a wide range of laser powers and scanning speeds. The surface of the single tracks was analysed for continuity and discontinuity after which the cross-section of the sintered tracks was also analysed. Generally, the geometry of the track's characteristics (width, height, and penetration depth) were determined by the laser powers and scanning speeds while the complete or partial melting of the powder particles was influenced by the powder particle size. The laser power of 150 W with a corresponding scanning speed of 1.0 m/s emerged as the optimum process parameter.

KEYWORDS: LPBF, Ti15Mo, single tracks, conduction mode and keyhole mode

INTRODUCTION

Laser powder bed fusion (LPBF) is an additive manufacturing process that uses a laser beam to melt powder particles to produce 3D structures layer-by-layer directly from a 3D CAD model. The CAD model is generated by a computerized system and based on the information on the CAD, a computer-controlled laser beam selectively scans the powder bed accordingly and fused the powder particles. The process begins with a laser beam scanning over a layer of powder and melts the powder particles under the beam and creates a small molten pool of metal [1]. As the laser beam traverses, it leaves a thin track of solidified metal behind known as a single track. It is the side by side arrangement of single tracks that would result in the production of single layers and the subsequent 3D objects. The quality of the individual set of single tracks determined the morphology and mechanical properties of the final 3D object [2].

Due to the unique potential offered by the LPBF technology to create 3D structures layer-by-layer, complex geometries can be easily optimized and produced monolithically. The LPBF technology can be used to produced intricate near-net-shape monolithically as opposed to the subtractive, multiply assembly steps used by the conventional methods (Turning, milling, grinding, drilling, etc.) of manufacturing [3]. The monolithic manufacturing of near-net-shape from single tracks layer-by-layer would translate into a reduction in manufacturing time, reduce assembling and maintenance cost, avoid waste of manufacturing materials, improved performance reliability and weight reduction [4-5]. The reduction in weight implies less fuel and emission of NOx for automotive (cars, aircraft, rockets, submarines, etc.) [4].

The layer-wise manufacturing process used by the LPBF technology has led futurists and researchers to predicted that different elemental powder could be in-situ alloyed with tailored properties, such as; thermal barrier coatings, thermal conductivity in conformal cooling channels, high hardness, and high-temperature resistance properties in turbines engines, optical properties in laser telecommunication systems; dielectric and magnetic properties in antenna and meta-materials; inclusion of embedded components such as resistors, sensors in electrical devices; increasing the lifetime and efficiency of tools in abrasive wear environment by combing hot work steel and tungsten carbide/cobalt, etc. via in-situ alloying [5-6].

The predictions of the futurist and researchers were made in lieu of the fact that the optimum process parameters for producing the basic unit blocks (single tracks) can be obtained experimentally for each type of powder composition such as the Ti15Mo been investigated in the current experiment. The literature has revealed the effort of many researchers in-situ alloying different elemental powders in different compositions to produce 3D objects with tailored mechanical properties for a specific application [7-9]. However, according to the review publication of Spears and Gold, there are more than 50 process parameters that governed the geometry and morphology of a single track [10]. Nonetheless, the hierarchical design principles of Yadroitsev et al. pointed out that laser power, spot size, and scanning speed are the main process parameters that determined the energy input and the interaction time between the laser beam and the powder bed [2]. These principal process parameters interactively have decisive effects on the geometry of a single track. The current research would focus on the laser power, scanning speed, and the powder particle size effect on the track's characteristics of the Ti15Mo powder blend.

The Ti15Mo is a generic alloy that has been around for a long time, however, unlike the well-celebrated Ti6Al4V that had widespread applications in the engineering and biomedical industries the Ti15Mo did not have much engineering applications. Notwithstanding, it had some applications in the medical and surgical devices industries [11]. According to Jablokov, et al. "the physical metallurgy of the alloy and the inability of the then-current reactive metals melting and processing machinery to handle this unusual binary alloy" had limit the widespread application of the Ti15Mo alloy [12]. The inherent limitations of the conventional methods (vacuum arc melting process, vacuum induction melting) of manufacturing the Ti15Mo alloy had adverse effects on the alloy. Producing the alloy with conventional methods lead to inhomogeneous microstructure, porosity, shrinkage, etc. Such defects have a direct decisive effect on the mechanical properties of the Ti15Mo alloy [13].

It is envisaged that with the unique versatility of the LPBF manufacturing processes, it would be possible to produce the Ti15Mo alloy without the above-mentioned defects, leading to the production of Ti15Mo alloy with improved mechanical properties [14]. It is, therefore, paramount to determine the optimum process parameters that could be used to produce the single tracks which would subsequently be used to manufacture the Ti15Mo alloy 3D structures layer-by-layer with the expected improved mechanical properties. Certainly, the current study will provide further insights into the understanding of the LPBF manufacturing process, increase the material data based for AM and the method used for determining the optimum process parameters for the Ti15Mo single tracks could be applied in the determination of optimum process parameters for other metallic powder compositions.

MATERIALS AND METHODS

Materials

Gas atomized spherical CpTi grade 2 and Mo supplied by TLS Technik GmbH was used for the experiment. The powder characterizations were specified by the supplier. The 10th, 50th and 90th percentiles of equivalent diameter (weighted by volume) of the CpTi powder particles were d_{10}=11.6 µm, d_{50}=24.6 µm, and d_{90}=38.4 µm. The percentiles equivalent diameter of the Mo powder was d_{10}=10.9 µm, d_{50}=22.4 µm, and d_{90}=31.9 µm. The chemical composition of the Ti is presented in table 1, and Mo is 99.9 % pure. 15 wt.% of Mo was mechanically mixed with 85 wt.% of the CpTi powder until a homogenous mixture was obtained. The mixture of Ti15%Mo was dried in an oven for about 15 hours at a temperature of 85 ^{0}C. The powder was stirred at 30 minutes interval.

Table 1. Ti powder chemical composition

Element	Ti	o	Fe	C	H	N
Content wt.%	Bal	0.17	0.062	0.006	0.002	0.012

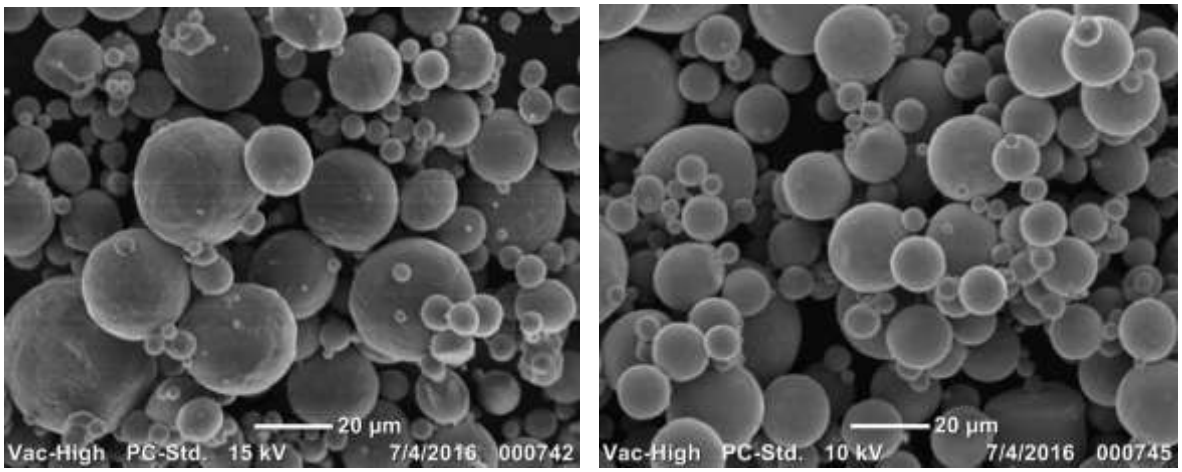

(a) (b)

Figure 1. SEM image of the supplied powders (A) CpTi (B) Mo

Production of the single tracks

The Electro-Optical System (EOS M280), a direct metal laser sintering (DMLS) machine was used for producing the single tracks. The laser spot diameter was 80 µm. Argon was used as a protective atmosphere. CpTi substrate was used and the powder layer thickness was 30 µm. The experiment was performed with multiple combinations of laser powers and scan speeds (Table 2) to produce the single tracks. All the tracks were of length 20 mm (Figure 2). Three single scan lines were produced for each scanning speed. For each laser power, the scanning speeds were of different incremental steps (Table 2). A space of 1.0 mm was placed between adjacent single tracks to avoid any interaction between neighboring scan tracks.

Table 2. Laser power and scanning speeds at various incremental steps

Factor	**Level**			
Laser power (W)	50	100	150	200
Scanning speed (m/s)	0.08 – 0.18	0.4 – 0.9	0.6 – 1.6	0.8 – 1.8
Incremental steps	0.02	0.1	0.2	0.2

Optical microscopy

The top surface of the sintered tracks was examined under an optical microscope after which the substrate (build plate) was section for the cross-sectional analysis. The cross-sections of the single tracks were metallurgically prepared based on the Struss protocol for Ti-based alloys [15]. The geometrical features in terms of the depth, width, and height of each of the single tracks were measured with A ZEISS Axio Scope.A1 optical microscope using Axio Vision SE64 software. Kroll enchant was used to etch the cross-sections of the single tracks to reveal the microstructure.

RESULTS AND DISCUSSIONS

The top surface analysis of the single tracks

During the LPBF process as the laser beam radiate the powder particles on the powder bed, the heat melts the powder at the top surface then penetrates the core of the remaining powder on the powder bed. The temperature within the powder bed becomes homogenize and a cylindrical molten pool is formed (Figure 2). Due to the multiple scattering, laser absorption by metal powders is significantly larger than the solid material [16]. The thermal conductively of the powder particles delivered on to the powder bed govern the laser-material interactions. The

thermophysical properties (absorptivity, specific heat capacity, thermal conductivity, density, coefficient of thermal expansion, and phase and state transformation temperatures) of the powder particle and the powder particle characteristics (size and distribution) influences the flow dynamics of the molten pool. The thermophysical properties (heat and radiation transfer) determined if the laser beam would be absorbed, reflected, or transmitted [17]. The influences of the thermophysical properties and the non-uniform distribution of the Gaussian laser beam that melt the powder particles trigger temperature gradient in the molten pool which induces surface tension in the molten pool [18]. Due to the surface tension, the molten fluid flows from the center of the melt pool to the edges of the melt pool in what is known as the Marangoni flow [18]. Marangoni flow is the dominant mechanism of convection (stirring effect) in laser-induced melt pools. It is the combination of these interactions (laser power, scanning speeds, thermophysical properties of the powder, Marangoni effect, powder particle size, etc.) that determined the melting, homogeneity, and the geometry of the single tracks. Chevron pattern (Figure 2) can be observed from the laser scanning direction because of the surface tension within the molten pool (Marangoni effect). The surface tensions cause the molten pool to oscillate resulting in the chevron pattern created as the molten pool solidified [17].

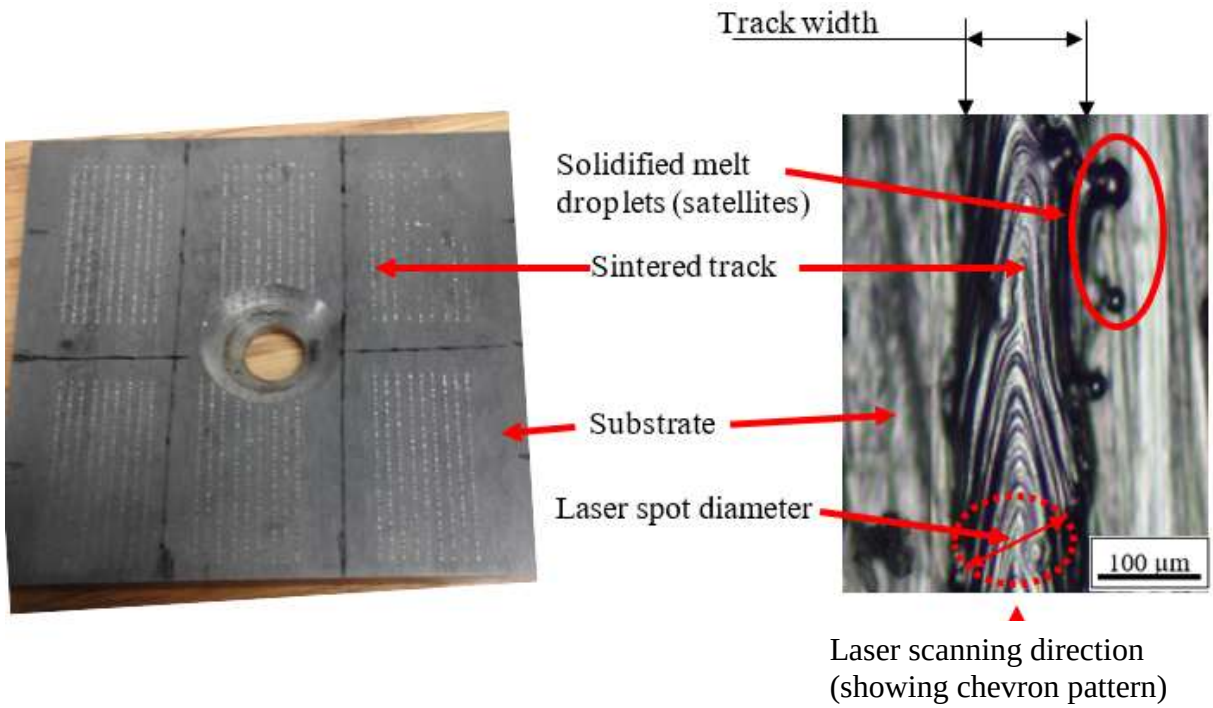

Figure 2. Top view of the substrate and the single tracks.

The geometry of the sintered track could be continuous, discontinuous, or balling (Table 4). Continuous tracks form when the combination of the selected process parameters can melt the powder mixture and produced tracks that exhibit continuous and consistent track width, while discontinuous tracks exhibit irregular tracks width. The balling and pre-balling (long beads) occur when the combination of the process parameters melts the powder and the cylindrical liquid breaks into balls (droplets) or beginning to break into long beads, commonly known as pre-balling effect [8,19]. The breaking of the cylindrical liquid (single tracks) occurs when the ratio of its length L to diameter W exceeds unity [20]. This implies that liquid cylinders with a high aspect ratio would break down to lower their surface energy. This phenomenon of cylindrical liquids breaking down into droplets to lower their surface energy is known as the Plateau-Rayleigh effect [20].

Generally, for all the sleeted laser powers the tracks geometry were continuous at the low scanning speeds (50 W - 0.08, 0.1 m/s; 100 W – 0.4, 0.5, 0.6 m/s; 150 W – 0.6. 0.8, 1.0, 1.2 m/s and 200 W – 0.8, 1.0 m/s) (Table 4). As the

scanning speeds begin to increase (50 W – 0.12 – 0.18 m/s; 100 W – 0.7 – 0.9 m/s; 150 W – 1.4 – 1.8 m/s and 200 W – 1.2 – 1.8 m/s) the laser energy fails to create continuous and consistent single tracks. This variation in the geometry of the tracks continues with increasing scanning speeds until the molten cylindrical liquids become very irregular and thin (pre-balling) (Table 4). The linear energy density (P/V) increases with decreasing scanning speeds [8]. Hence at low scanning speeds, the laser energy was able to melt the Ti15Mo powder particles and formed continuous tracks. The laser beam dwells longer at a particular spot on the powder bed at low scanning speeds and melt the powder completely and formed continuous tracks. As the scanning speeds increases the linear energy (P/V) decreases, and the temperature in the molten pool falls. The low temperature (less laser energy) fails to melt the powder completely and formed discontinuous tracks as the scanning speeds increases.

During the melting process, the laser beam does not melt only the powder on its path, but also powder particles close to the edge of the laser beam (Figure 2- satellites). Melting of powders in the peripheral of the laser beam may result in imperfect or incomplete powder melting since the laser energy transfer to powder particles outside the margin of the laser spot is insufficient to melt the powder completely. The partially melted powder particles in the proximity of the laser beam were sintered to the solidified melt pool (Figure 2). It is the same phenomenon of the laser beam melting of powder particles in the peripheral zone of the laser beam that causes denudation effects [2]. It is a situation whereby the first and the last tracks are higher than the other tracks, because of the involvement of powders from the edge of the laser spot into the molten pool thereby reducing the consolidated zone and causes other tracks to be smaller in size. Both satellites and denudation effects could lead to pore formation which can affect the mechanical properties of LPBF built parts [2].

Cross-section analysis of the single tracks

The cohesion (welding) between successive layers plays an important role in the mechanical properties of LPBF parts. The penetration depth determines the cohesion between the successive layers. The penetration depth, in this case, refers to the depth of penetration into the substrate material - previously sintered layer (re-melted depth). According to Yadroitsev, et al., each synthesized layer must penetrate the layer below enough to successfully produce consolidated single tracks [2]. After the top view analysis of the single tracks, the substrate was section into pieces to examine the geometry of the single tracks from the cross-sectional view of the plates.

At low laser power of 50 W and low scanning speeds (0.08, 0.1 m/s), the effective energy transferred to the powder bed was able to melt the Ti15Mo powder completely and formed nearly a homogenous alloy of Ti15Mo matrix (Table 4). The effective energy transferred is defined as the ratio between the laser energy absorbed by the target material and the originally irradiated laser power [21]. However, the energy density was not enough to penetrate the substrate to form a strong "welding" with the substrate (the previous layer) (Table 4). As the laser scanning speeds increase (0.12, 0.14, 0.16, 0.18 m/s) at a constant laser power of 50 W the geometry of the single tracks started becoming irregular in shape and the powder particles also begin to melt incompletely (Table 4).

As the scanning speed increases the temperature within the molten pool begins to decrease because the linear energy density decreases with increasing scanning speeds. The low temperature in the molten pool could only melt the Ti powder particles completely and Mo powder particles partially. The partially melting of Mo is due to the thermophysical differences between the two materials (Table 3). The melting point of Mo is about 1000 ^{0}C higher than that of Ti, hence the low temperature in the molten pool was enough to melt the Ti but insufficient to melt Mo as the scanning speeds increase. The laser reflectance of Mo is higher than that of Ti, hence Ti would absorb more laser energy while Mo would reflect more of the laser radiation, hence Ti was able to melt at the low temperature in the molten pool [22]. Also, the density of Mo is higher than that of Ti (Table 3), therefore during the LPBF melting process, the Mo sink to the bottom of the molten pool and was shielded from the full intensity of the laser radiation and could not melt completely. Although the thermal conductivity of Mo is very high as compared to Ti (Table 3), the high rate of the heating and cooling manufacturing process of the LPBF technology could not permit Mo to melt completely before the solidification process. If the rate of melting and solidification of the molten pool could be

controlled to occurs slowly, perhaps all the Mo could have melted before the solidification due to its high thermal conductivity.

It is worth mentioning that, measuring the size of the partially melted Mo particles (< 20 microns) embedded in the Ti15Mo matrix after the LPBF process, indicated that the Ti15Mo matrix was not formed by liquid phase sintering and partial diffusion bonding at the Mo particle surface with the Ti, but by the complete melting of the Ti and smaller Mo powder particles as well as the partial melting of the larger Mo powder particles (Figure 1). For all the laser powers the quantity of the partially melted Mo particles increases with increasing scanning speeds due to the reduction of the temperature in the molten pool with increasing scanning speeds.

Table 3. Thermophysical properties of Ti and Mo [24]

Thermophysical properties	CpTi	Mo
Melting point, ^{o}C	1668	2617
Density, Kgm^{-3}	4500	10220
Specific heat capacity J·kg^{-1}K^{-1}	528	276
Thermal conductivity, Wm^{-1}K^{-1}	17	138

It is very important to point out that the large energy density (P/V) of 625 J/m at the laser power of 50 W with the corresponding scanning speed of 0.08 m/s could not melt the substrate (the previous layer – Table 4). This shows that it is not about the value of the linear energy density but a careful combination of the process parameters that could yield optimum results.

Table 4. Morphology and geometry of the single tracks

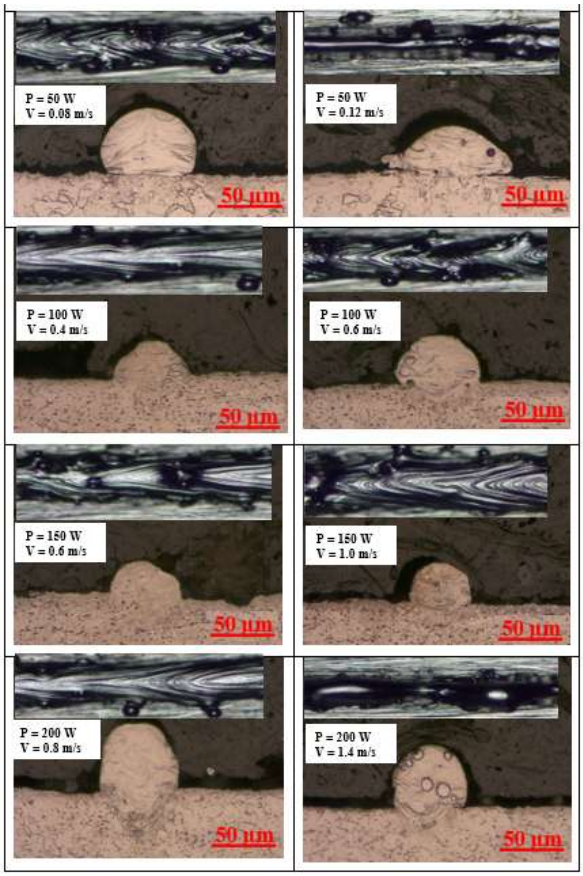

Similar to what was observed at the laser power of 50 W, for single tracks produced at laser powers of 100 W, 150 W and 200 W the laser energy densities were able to melt the Ti15Mo powder particles completely at low scanning speeds (100 W – 0.4, 0.5, 0.6 m/s; 150 W – 0.6. 0.8, 1.0, 1.2 m/s and 200 W – 0.8, 1.0 m/s). As the scanning speeds beginning to increase the laser energy was not sufficient to melt the Mo powder particles complete and the amount of partially melted Mo particles increase with increasing scanning speeds. The mixing (homogeneity) of the molten pool also decrease with increasing scanning speeds due to the reduction in the convective flow (high viscous melt flow) in the molten pool at low temperature. The geometry of the tracks generally becomes more irregular with increasing scanning speeds

At 100 W the effective linear energy was able to melt the substrate (the previous layer). However, the penetration was shallow and might not result in building a dense (non-porous) 3D objects due to the layer-wise process of production. The penetration depths of the single tracks at the laser power of 150 W begin to resemble a bowl shape (spherical shape) especially for single tracks produced at 1.0 m/s (Table 4). Such "U" shape penetration into the substrate is normally considered as the optimum, and the combination of the process parameters that yield such a result is called optimum process parameters (conduction mode) [17].

At higher laser power of 200 W at low scanning speeds of 0.8 m/s and 1.0 m/s, the laser energy melts the powder completely and continues to melt the substrates very deed forming a dagger-like penetration into the substrate (Table 4). The combination of process parameters that produce single tracks with such deep penetrations are not desirable for additive manufacturing. The high energy density could have caused the Ti15Mo powder particles to melt and vaporize in some local regions within the molten pool. Due to the rapid hydrodynamic movement of the melt flow, the vapour may not be able to escape and could be become entrapped in the solidified melt pool which can lead to pore formation. However due to the thermal recycling when building 3D objects the entrap gas at the top of a solidified metal can escape out of the layer during subsequent layer deposition. The pores formed deep inside, and in the lower end of the melt pool, are more detrimental [17].

However, no pores were observed in the deep penetration zone of the single tracks produces in the current experiment. This might be attributed to the effect of the larger Mo powder particle size. The density of Mo is higher than that of Ti, hence it sinks to the bottom of the molten pool during the melting process. As the laser beam radiates the powder bed and melts the Ti15Mo powder before continuing with the melting of the substrate, the larger Mo particles at the bottom of the melt pool absorbed most of the laser energy. Therefore, acting as a shield for the substrate (the previous layer) hence not much of the laser energy was absorbed into the base plate during the deep melting process. This explanation was not given in the authors previous paper which set the tone for the current investigations [23]. No pore was found in the deep penetration zone in the current experiment. Probably increasing the laser power more than 200 W could lead to pore formation in the deep zone at low scanning speeds. Such deep penetration is termed in the litterateur as a keyhole [21].

Zhao, et al. explained that keyhole mode occurs if the energy transfer efficiency is larger than the material's absorptivity due to high reflectivity and thermal conductivity within the melt pool while conduction mode occurs if the energy transfer efficiency is equal to the material's absorptivity [21]. For a conduction mode, the depth of penetration should not be more than half the width of the track [21]. As presented in Table 4 the tracks produced at 50 W have almost zero penetration and tracks at 100 W also did not have sufficient penetration depth. The average widths of the tracks produced at 150 W at low scanning speeds of 0.6 – 1.2 m/s measured from the widest region of the melt pool ranges from 95±4 – 72±3 µm whiles the penetration depths range from 65±5 – 56±7 µm representing the window of conduction mode. The geometry of the single track at a scanning speed of 1.0 m/s has the most ideal characteristics that defined an optimum process parameter, hence laser power of 150 W with a corresponding scanning speed of 1.0 m/s is recorded as the optimum process parameter [25].

The average widths of single tracks produce at low scanning speeds of 0.8 and 1.0 m/s at the laser power of 200 W was 99±4 µm. The average overall height of the scan tracks (including both the depth of penetration below the substrate surface and the height above the substrate surface) at the 200 W was 218±7 µm. The larger depth of the

melt pool compared to its width indicates keyhole mode melting rather than conduction mode melting. All the other sintered tracks at high scanning speeds (150 W – 1.4, 1.6 m/s; 200 W – 1.2, 1.4, 1.6. 1.8 m/s) produced tracks with irregular geometry (Table 4). Generally, it could be concluded that the depth and width of a melt pool are controlled by the laser power and the scan speed while the size of the powder particles determined the complete or partial melting of the powder particles.

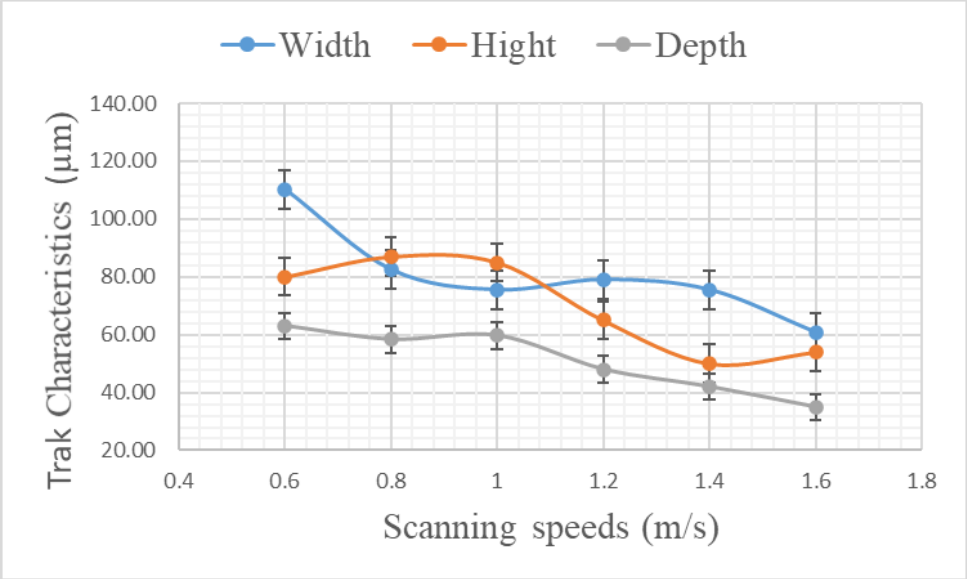

Figure 3. Tracks characteristics at 150 W as a function of scanning speeds

For all the combination of process parameters the track's characteristics (width, height, and penetration depth) decrease with increasing scanning speeds (Figure 3) at constant laser powers. The high temperature within the molten pool at low scanning speeds produces a large liquid phase with low viscosity. The large liquid phase enhances the prominent flow of the molten pool which leads to the increase of the widths of the tracks with decreasing scanning speeds. The deep penetration depth is the result of continued absorption of the laser radiation at a particular spot on the powder bed at low scanning speeds due to the increased dwelling time of the laser beam at a spot. The corrugated nature of the height of the tracks is due to the non-uniform nature of the Gaussian laser beam that melts the metallic powders. The non-uniform distribution of the Gaussian beam creates non-uniform temperatures distribution within the molten pool resulting in a temperature gradient [18]. The temperature gradient triggers oscillation (ripple) of the molten pool, leading to a solidified molten pool of uneven surface. The uneven surface of the solidified molten pool could lead to pore formation in the 3D manufactured part. If the surface of the previous layer is not even, it could lead to uneven powder deposition on the powder bed for the subsequent layers which would cause inconsistent melting. The inconsistent melting can lead to micropores in the final 3D objects.

Table 5. Cross-section of the sieve and un-sieve single tracks

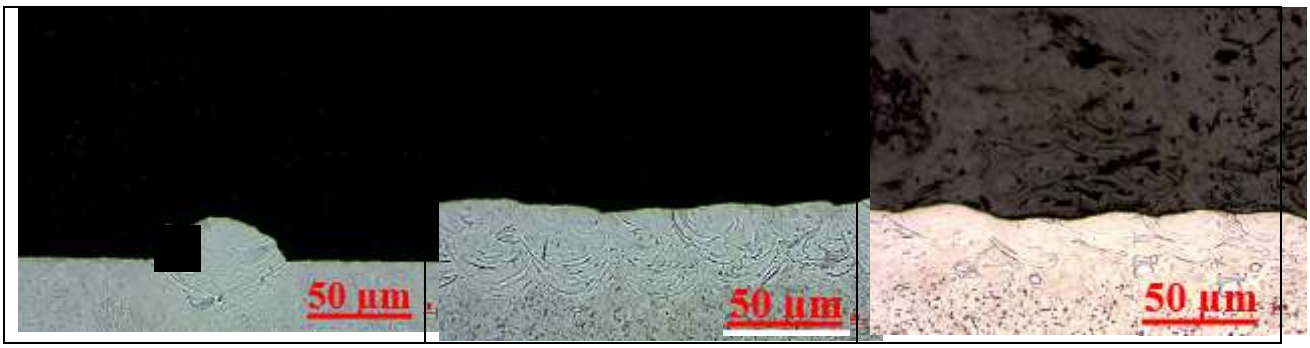

To ascertain the assertion that the laser energy delivered on the powder bed was able to melt the Ti and the smaller Mo power particles completely, but melt the larger Mo powder particles partially; the Mo powder was sieved to particle size < 20 microns. 15 wt.% of the sieved Mo powder was mechanically mixed with the 85 wt.% of the CpTi powder. The optimum scanning speed (1.0 m/s) already determined at the laser power of 150 W was used to produce single tracks with the new sieved powder. As envisaged the Mo powder particles melt completely (Table 5) and there was a very good dispersion of the alloying element (Mo) within the base metal (Ti). It is now empirically proven that the laser energy melts the larger Mo powder particles partially when the un-sieve Mo powder was used and the process did not occur by liquid phase sintering and partial diffusion bonding at the Mo particle surface with the Ti. A single layer was produced at the optimum process parameters of 150 W at a scanning speed of 1.0 m/s using both un-sieve and sieve powder. The micrographs of the single layers reveal that all the Mo powder particles melt completely when the sieved powder was used and the alloying element (Mo) dispersed evenly in the based metal (Ti) whiles the larger Mo particles remain partially melted when the un-sieve powder was used.

CONCLUSION

Optimum process parameters for the Ti15Mo powder blend was determined through in situ alloying using the LPBF manufacturing process. It was concluded that laser power, scanning speed and powder particle size distribution generally have a decisive effect on the morphology, geometry, melting and the homogeneity of the Ti15Mo tracks matrix. The top surface of the sintered tracks reveals that the widths of the tracks decrease with increasing scanning speeds. Also, the cross-sectional analysis reveals that the penetration depth of the tracks decreases with increasing scanning speeds. The heights of the tracks were irregular which was attributed to the non-uniform distribution of the Gaussian laser beam that melts the Ti15Mo powder particles.

ACKNOWLEDGMENT

This work is based on the research supported by the South African Research Chairs Initiative of the Department of Science and Technology and National Research Foundation of South Africa (Grant №97994). The author would like to acknowledge the contribution of Prof. I. Yadroitsau, Prof. P. Krakhmalev and Dr. I. Yadroitsava who were his doctoral studies supervisors.

REFERENCES

[1] J.C. Najmon, S. Raeisi and A. Tovar, "Review of additive manufacturing technologies and applications in the aerospace industry," In Additive manufacturing for the aerospace industry, Pp. 7-31, 2019.

[2] I. Yadroitsev, P. Krakhmalev and I. Yadroitsava, "Hierarchical design principles of selective laser melting for high quality metallic objects," Additive Manufacturing, Vol. 7, Pp. 45-56, 2015.

[3] T.C. Dzogbewu, "Additive manufacturing of porous Ti-based alloys for biomedical applications–a review," Journal for New Generation Sciences, Vol. 15, No. 1, Pp. 278-294, 2017.

[4] B.P. Bewlay, M. Weimer, T. Kelly, A. Suzuki and P.R. Subramanian, "The science, technology, and implementation of TiAl alloys in commercial aircraft engines," MRS Online Proceedings Library Archive, 1516, Pp. 49-58, 2013.

[5] R. Jiang, R. Kleer and F.T. Piller, "Predicting the future of additive manufacturing: A Delphi study on economic and societal implications of 3D printing for 2030," Technological Forecasting and Social Change, Vol. 117, Pp. 84-97, 2017.

[6] M. Vaezi, S. Chianrabutra, B. Mellor and S. Yang, "Multiple material additive manufacturing–Part 1: a review," Virtual and Physical Prototyping, Vol. 8, No. 1, Pp. 19-50, 2013.

[7] A. Kinnear, T.C. Dzogbewu, I. Yadroitsev, P. Krakhmalev and I. Yadroitsava, "Manufacturing, microstructure and mechanical properties of selective laser melted Ti6Al4V-Cu," in LiM" Lasers in manufacturing" conference, Munich, 2017.

[8] A. Zenani, T.C. Dzogbewu, W.B. Du Preez and I. Yadroitsev, "Optimum Process Parameters for Direct Metal Laser Sintering of Ti6Al Powder Blend," Universal journal of mechanical engineering, Vol. 8, No. 4, Pp. 170-182, 2020.

[9] S. Dadbakhsh, R. Mertens, L. Hao, J. Van Humbeeck and J.P. Kruth, "Selective laser melting to manufacture "in situ" metal matrix composites: A review," Advanced Engineering Materials, Vol. 21, No. 3, Pp. 1801244, 2019.

[10] T.G. Spears and S.A. Gold, "In-process sensing in selective laser melting (SLM) additive manufacturing," Integrating Materials and Manufacturing Innovation, Vol. 5, No. 1, Pp. 1-25, 2016.

[11] M. Niinomi, "Mechanical properties of biomedical titanium alloys," Materials Science and Engineering: A, Vol. 243, No. 1, Pp. 231-236, 1998.

[12] V.R. Jablokov, M.J. Nutt, M.E. Richelsoph and H.L. Freese, "The application of Ti-15Mo beta titanium alloy in high strength structural orthopaedic applications," In Titanium, Niobium, Zirconium, and Tantalum for Medical and Surgical Applications, Journal of ASTM International, Vol. 2, No. 8, 2006.

[13] L.E. Murr, S.M. Gaytan, F. Medina, H. Lopez, E. Martinez, B.I. Machado, D.H. Hernandez, L. Martinez, M.I. Lopez, R.B. Wicker and J. Bracke, "Next-generation biomedical implants using additive manufacturing of complex, cellular and functionnal mesh arrays," Philosophical Transactions of the Royal Society A: Mathematical, Physical and Engineering Sciences, Vol. 368, No. 1917, Pp. 1999-2032, 2010.

[14] B.R.E.N.T. Stucker, "Additive manufacturing technologies: technology introduction and business implications.," 2012.

[15] L. Bjerregaard, B. Geels, M. Ottesen and M. Ruckert, Metalog Guide, Struers A/S, 1996.

[16] C.D. Boley, S.A. Khairallah and A. Rubenchik, "Calculation of laser absorption by metal powders in additive manufacturing," Applied Optics, Vol. 54, No. 9, Pp. 2477-2482, 2015.

[17] J. Ion, "Laser processing of engineering materials: principles, procedure and industrial application," Elsevier, 2005.

[18] S. Kou, C. Limmaneevichitr and P.S. Wei, "Oscillatory Marangoni flow: a fundamental study by conduction-mode laser spot welding," Welding Journal, Vol. 90, No. 12, Pp. 229-240, 2011.

[19] J.J.S. Dilip, S. Zhang, C. Teng, K. Zeng, C. Robinson, D. Pal and B. Stucker, "Influence of processing parameters on the evolution of melt pool, porosity, and microstructures in Ti-6Al-4V alloy parts fabricated by selective laser melting," Progress in Additive Manufacturing, Vol. 2, No. 3, Pp. 157-167, 2017.

[20] S. Chandrasekar, Hydrodynamic and Hydromagnetic Stability, New York: Clarendon Press, Oxford, 1961.

[21] H. Zhao, D.R. White and T. DebRoy, "Current issues and problems in laser welding of automotive aluminium alloys," International materials reviews, Vol. 44, No. 6, Pp. 238-266, 1999.

[22] D.W. Lynch, W.R. Hunter and E.D. Palik, Handbook of optical constants of solids, Orlando: Academic press, 1985.

[23] T.C. Dzogbewu, I. Yadroitsev, P. Krakhmalev, I. Yadroitsava, A. Du Plessis, Optimal process parameters for in-situ alloyed Ti15Mo structures by Direct Metal Laser Sintering. In SSF 2017-The 28th Annual International Solid Freeform Fabrication Symposium, Austin, No. 7-9, Pp. 75-96, 2017.

[24] MatWeb, "Material property data," 2016. [Online]. Available: http://www.matweb.com. [Accessed 12 February 2020].

[25] J. Yang, J. Han, H. Yu, J. Yin, M. Gao, Z. Wang and X. Zeng, "Role of molten pool mode on formability, microstructure and mechanical properties of selective laser melted Ti-6Al-4V alloy," Materials & Design, vol. 110, Pp. 558-570, 2016.